Monthly Notices of the ROYAL ASTRONOMICAL SOCIETY

MNRAS **504,** 1959–1968 (2021) doi:10.1093/mnras/stab1017
Advance Access publication 2021 April 14

Probing possible effects of circumgalactic media on the metal content of galaxies through the mass–metallicity relationship

Sai Zhai [1,2] Yong Shi [1,2]★ Jianhang Chen,[1,3] Longji Bing [1,4] Yanmei Chen,[1,2] Xiaoling Yu [1,2] and Songlin Li[1,2]

[1]*School of Astronomy and Space Science, Nanjing University, Nanjing 210093, China*
[2]*Key Laboratory of Modern Astronomy and Astrophysics (Nanjing University), Ministry of Education, Nanjing 210093, China*
[3]*European Southern Observatory, Karl-Schwarzschild-Strasse 2, D-85748 Garching bei Muenchen, Germany*
[4]*Aix Marseille Université, CNRS, CNES, LAM (Laboratoire d'Astrophysique de Marseille), F-13013 Marseille, France*

Accepted 2021 April 9. Received 2021 April 9; in original form 2020 November 9

ABSTRACT

The circumgalactic medium (CGM) connects the gas between the interstellar medium and the intergalactic medium, which plays an important role in galaxy evolution. We use the stellar mass–metallicity relationship to investigate whether sharing the CGM will affect the distribution of metals in galaxy pairs. The optical emission lines from the Sloan Digital Sky Survey Data Release are used to measure the gas-phase metallicity. We find that there is no significant difference in the distribution of the metallicity difference between two members in star forming–star forming pairs ($\Delta\log(O/H)_{diff}$), metallicity offset from the best-fitting stellar mass–metallicity relationship of galaxies in pairs ($\Delta\log(O/H)_{MS}$), as compared to 'fake' pairs. By looking at and as a function of the star formation rate (SFR), specific SFR, and stellar mass ratio, no difference is seen between galaxies in pairs and control galaxies. From our results, the share of the CGM may not play an important role in shaping the evolution of metal contents of galaxies.

Key words: galaxies: evolution; galaxies: star formation.

1 INTRODUCTION

Galaxies are surrounded by the multiphase gas: the circumgalactic medium (CGM), which extends beyond the interstellar medium (ISM) but within the virial radius (Tumlinson, Peeples & Werk 2017). Galactic scale outflow is common in the active star-forming (SF) galaxies (Weiner et al. 2009; Chen et al. 2010; Steidel et al. 2010), which drives the metals produced in the SF region to the CGM (Heckman, Armus & Miley 1990; Tumlinson et al. 2011). As a result, even though the CGM is diffuse and thin, it contains the same, or even more amount of baryons than the galaxy disc in spirals (Tumlinson et al. 2011; Lochhaas et al. 2020; Werk et al. 2014). Besides outflows, the galactic inflow/accretion of CGMs deposit fresh gas fuel for star formation in discs. This recycling of the material between CGM and discs through outflows and inflows/accretion is one of the key physical processes that shape galaxy formation and evolution (Tumlinson et al. 2017). In this study, we employ the mass–metallicity relationship to probe the possible effects of such recycling on galaxy evolution.

The correlation between the stellar mass-metallicity (hereafter MZR) is one of the most important relationships to study the formation and evolution of galaxies (Erb et al. 2006; Kirby et al. 2013). Stellar mass estimates the amount of gas that has turned into stars. Metal traces the star formation history (Zahid, Kewley & Bresolin 2011). The relationship between them can be used to study the physical processes related to the formation and distribution of metals.

The analysis of MZR starts from irregular, blue compact galaxies (Lequeux et al. 1979). The work by Tremonti et al. (2004) has used 53 000 SF galaxies to find a nice relationship between stellar mass and metallicity. The trend below $10^{10.5}$ $M_\odot$ is steep, and above $10^{10.5}$ $M_\odot$ becomes flat. They pointed out that galactic wind takes an important role in shaping the trend of the MZR. Over decades, studies of MZR have extended to high redshift (Troncoso et al. 2014; Yabe et al. 2014; Ly et al. 2016; Onodera et al. 2016; Sanders et al. 2018), dwarf galaxies (Lee et al. 2006; Blanc et al. 2019), and simulation (Brooks et al. 2007; Ma et al. 2015). Chisholm, Tremonti & Leitherer (2018) presents that in the local universe, outflow causes the loss of 78 per cent metal. However, the origin of the stellar mass–metallicity relationship is still uncertain. At least, four main physical processes affect the MZR: the low star formation efficiency of low stellar mass galaxies (Calura et al. 2009), the infall and outflow of unenriched/enriched gas (Finlator & Davé 2008; Garnett 2002), and variation of initial mass function under different physical conditions (Köppen, Weidner & Kroupa 2007; Mannucci et al. 2010).

Compared to isolated galaxies, galaxies in pairs may share a common CGM so that their evolution may be linked to some extent for the following reasons. First, galactic scale activities, such as outflow, inflow, accretion, and recycling occur in the region of the CGM, which regulates the distribution of gas and metal (Heckman et al. 1990; Tumlinson et al. 2011; Tumlinson et al. 2017). Secondly, the CGM contains the majority of baryon in the galaxy, which might provide material for star formation (Werk et al. 2014). Thirdly, for

★ E-mail: yong@nju.edu.cn

galaxies in pairs that also interact with each other, they already share the CGM to a degree and the interaction between them helps to regulate the distribution of gas and metal, which enhances the potential link. For example, Pan et al. (2018) finds that the interaction between pairs enhances the star formation rate (SFR). Satellite galaxies located in dense environments tend to hold more metals because the metal-rich gas from the high-density region enhances the metallicity of satellites (Peng & Maiolino 2014). In Kewley, Geller & Barton (2006), they show that the merging process triggers the infall of metal-poor gas, thus decreasing the metallicity in the central regions of galaxies.

In this paper, we search for the metallicity difference between galaxy pairs, which may shed light on the roles of CGMs in driving galaxy formation and evolution. To differentiate the effect of galaxy interaction from that of sharing CGM in affecting the metals of galaxies, we expand the definition of pairs to be those with separations < 300 kpc and choose 150 kpc (Bustamante et al. 2020) as the demarcation point to determine whether there is an interaction between pairs or not. In addition, besides SF–SF pairs), we add another type of galaxy pairs that contains one SF member galaxy and one passive member galaxy (SF–Passive pairs), which has no CGM sharing. This is because passive galaxies contain less ionized gas in the CGM than SF galaxies (Tumlinson et al. 2011). Two important parameters are included to quantitatively measure the metallicity difference between pairs. One is the metallicity difference between two members in pairs ($\Delta\log(O/H)_{\rm diff}$, in equation 4), another is the metallicity offset from the best-fitting stellar mass–metallicity relationship of galaxies in pairs ($\Delta\log(O/H)_{\rm MS}$, in equation 5). We describe the observation and data reduction in Section 2. In Section 3, we show the MZR and metal difference of pairs from Sloan Digital Sky Survey Data Release (SDSS DR7). In Section 4, we discuss the incompleteness of the data and the physical mechanism. The conclusion is in Section 5. We adopt the flat ΛCDM model, $h = 0.677$, $\Omega_m = 0.307$ (Planck Collaboration 2016).

2 OBSERVATIONS AND DATA REDUCTION

The SDSS (York et al. 2000) uses the 2.5-m optical telescope located at Apache Point Observatory (Gunn et al. 2006), began in 2000, which aims to obtain the multispectral imaging, spectra of galaxies, and 10 000 quasars over 10 000 deg^2 of the sky. The SDSS DR7 provides such a large amount of samples to study the physical properties of the local universe. The optical emission line data are from SDSS DR7 (Abazajian et al. 2009) because this release consists of nearly 1 million spectra, which spans a wavelength coverage from 3800 to 9600 Å with a resolution of nearly 2000. Due to the reason that the diameter of each fiber is 3 arcsec, we only analyse the central region of galaxies. The redshift range of the galaxies we used in this paper is from 0.02 to 0.25, thus the size of the central region is from 1.36 to 14.86 kpc. Most have data within 5 kpc.

2.1 SF galaxies and passive galaxies

We use strong optical emission lines to calculate the metallicity, and remove the contributions from active galactic nucleus. Therefore, we focus on the SF galaxies. The BPT diagram (Baldwin, Phillips & Terlevich 1981) is exploited to select the SF galaxies, which requires that galaxies fall below the [N II]λ6584/Hα versus [O III]λ5007/Hβ diagram (Kewley et al. 2001; Kauffmann et al. 2003). The optical emission lines, the stellar mass (Kauffamnn et al. 2003; Salim at al. 2007), the specific SFR (sSFR), and SFR (Brinchmann et al. 2004) for SDSS DR7 galaxies are from the MPA-JHU[1] catalogue. After removing galaxies with unreliable emission lines (SNR ≤ 5), we found 68 355 SF galaxies in the SDSS DR7 catalogue. We use the definition of passive galaxies (sSFR $\leq 10^{-11}$ yr^{-1}) from Tumlinson et al. (2011).

Table 1. Conditions of different types of pairs.

Type of pairs	Projected distance	
	Less than 150 kpc	Between 150 and 300 kpc
SF–SF pairs	Interaction and CGM sharing	No interaction but with CGM sharing
SF–passive pairs	Interaction and without CGM sharing	No interaction and without CGM sharing

2.2 Pair galaxies and match to controls

Pair galaxies are selected using the following criteria: the projected separation between galaxies need to be less than 300 kpc and larger than 7.21 kpc (Patton & Atfield 2008); the line-of-sight velocity difference $|\Delta V| < 1000$ km/s (Wilson et al. 2019); at least one neighbourr was observed by SDSS DR7. The minimum separation is used to remove the case that the very close galaxy pairs are mistakenly classified as a single galaxy (Patton & Atfield 2008).

This work is going to study the CGM surrounding galaxies in pairs, not only the interaction between galaxies. Therefore, as long as two galaxies share some overlap of their CGMs, we can use them no matter they are interacting with each other or not. Since Tumlinson et al. (2011) detected CGM out to 150 kpc for a galaxy and Wilde et al. (2020) found that the radius of CGM is larger than 150 kpc, so we can select a galaxy pair with a separation smaller than 300 kpc. Here, we assume that galaxies with separation smaller than 300 kpc have somewhat overlapped CGMs. We finally find 4297 SF–SF pairs and 12 254 SF–passive pairs. The SF–passive pairs only have interaction but no CGM sharing, which will be used to understand the effect of CGM sharing in the SF–SF pairs. The conditons of pairs are shown in Table 1.

The projected distance distribution and the stellar mass ratio are shown in Fig. 1. The red vertical line in the top panel is used to guide our eyes to show that we indeed remove the pairs with separation less than 7.21 kpc. For both SF–SF pairs and SF–passive pairs, when the projected distances of pairs are smaller than 100 kpc, there are more pairs with increasing separation. However, for SF–SF pairs, the separation seems to be evenly distributed when it is larger than 100 kpc. Most of the SF–SF pairs have equal stellar masses. But for SF–passive pairs, most of them are unequal in stellar masses.

After removing pair galaxies from the whole sample of star forming galaxies, we have 24 586 isolated galaxies left for the control pool. Following the method in Patton et al. (2016), we select five control galaxies from the control pool with similar stellar mass (0.1 dex) and redshift (0.01) for each SF galaxy in pairs. Because of the span of these two parameters, a weighting scheme is needed to quantify the matches of pairs and control samples. Thus, two parts should be taken into account when calculating the overall weight: one for redshift weight and another for stellar mass

[1]https://wwwmpa.mpa-garching.mpg.de/SDSS/DR7/, Charlot S., Kauffmann G., (MPA) S. W., (JHU) T. H., TremontiC., Brinchmann J., Leidel S., 2010, The MPA-JHU DR7 release of spectrum measurements

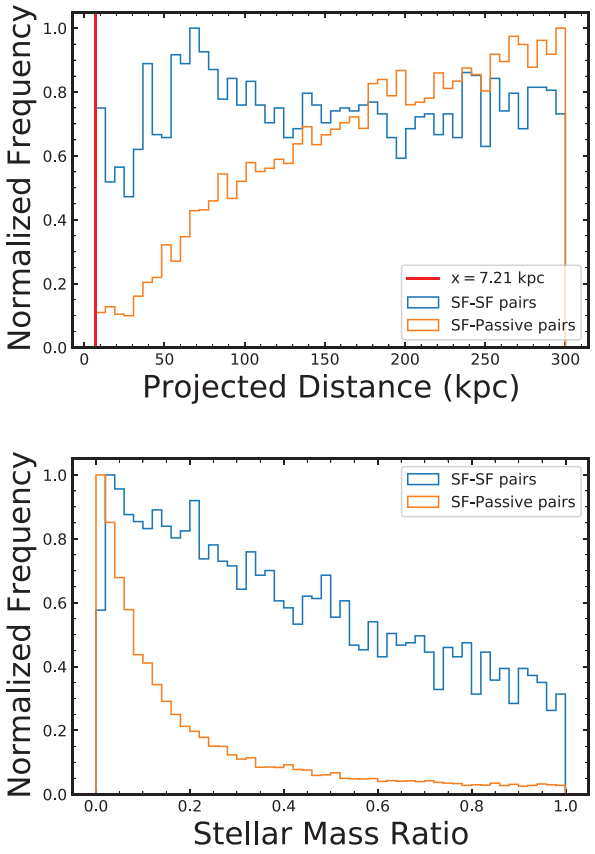

Figure 1. The normalized frequency distribution of the separation and the stellar mass ratio for pairs from the SDSS DR7 are shown in this figure. The red vertical line in the top panel represents the projected distance between pairs equals to 7.21 kpc. The blue, orange colour show the SF–SF pairs, SF–passive pairs, respectively.

weight. The $i-th$ overall weight of the control sample is defined as:

$$w_i = w_{z_i} * w_{M_i}, \tag{1}$$

where w_{z_i} and w_{M_i} represent the redshift weight and the stellar mass weight, respectively. The redshift weight is defined as:

$$w_{z_i} = 1 - \frac{|z - z_i|}{z_{tol}}, \tag{2}$$

where z, z_i, and $z_{tol} = 0.01$ are the redshift of pair galaxy, the redshift of $i-th$ control samples of each pair, and the redshift tolerance. The stellar mass weight is defined as:

$$w_{M_i} = 1 - \frac{|log(M) - log(M_i)|}{M_{tol}}, \tag{3}$$

where M, M_i, and $M_{tol} = 0.01$ are the stellar mass of pair galaxy, the stellar mass of $i-th$ control samples of each pair, and the stellar mass tolerance.

2.3 Balmer decrement and dust extinction correction

Dust extinction will occur when the light comes through the dust. The scatter and absorption of dust follow this rule: the light with a shorter wavelength will be extincted more than that with a longer wavelength (Mathis 1990). Generally, the Balmer decrement, which is the higher-order Balmer emission line flux relative to Hβ (Savaglio et al. 2005), is accepted to correct this effect. In this paper, we choose the ratio of Hα and Hβ. In the Case B situation, where the temperature is 10^4 K, the theoretical Hα/Hβ is 2.86 for the electron densities $n_e = 10^2$ cm^{-3} (Groves, Brinchmann & Walcher 2012). Because two emission lines are close in wavelength, the difference of dust emission is so small that we can ignore it when selecting SF galaxies. Therefore, with the Balmer decrement, the equation between the intrinsic flux and the observed flux, the reddening curve from Calzetti et al. (2000), we obtain the intrinsic flux for other optical emission lines of SF galaxies, such as [N II]λ6584, Hα, [O III]λ5007, Hβ.

2.4 Metallicity indicator

The most reliable way to obtain metallicity is to directly measure the electron temperature of gas (Kewley & Ellison 2008). They use the ratio between [O III]λ4363 and other low-ionization emission lines such as [O III]λ5007. However, [O III]λ4363 usually exists in the metal-poor region of the galaxies and it is too weak to be observed (Garnett, Kennicutt & Bresolin 2004). Thus, other indicators are introduced to make up for these problems. For example, the classical method is based on the photoelectric model, and the method is based on the combination of the electron temperature and the photoelectric model. However, the photoelectric model is only suited for the geometrical spherical situation, which can not exist in the real universe environment (Kewley & Ellison 2008). Therefore, in this paper, we choose two metallicity indicators and cross-check the results.

One indicator from the photoionization model is KD02 (Kewley & Dopita 2002). It depends on the relationship between R_{23} = ([O II]λ3727 + [O III]$\lambda\lambda$4959, 5007)/Hβ and metallicity. R_{23} provides an estimation of the ratio of total cooling caused by oxygen. However, for this method, [N II] /[O II] are needed to break the degeneracy between R_{23} and metallicity. Another metallicity indicator D02 (Denicoló, Terlevich & Terlevich 2002) is derived by the monotonic relationship between logarithmic [N II]λ6584/Hα ratio and metallicity for 155 H II regions.

3 RESULTS

Fig. 2 shows the stellar mass–metallicity relationship of all SF galaxies and pair galaxies in the violin plot. Similar to the results from Tremonti et al. (2004), there is a tight relation between stellar mass and metallicity, showing a monotonic correlation and getting flat when stellar mass is higher than $10^{10.5}$ M$_\odot$. Overall, the metallicity from KD02 is larger than that of D02. This difference is introduced by the different calibration we used. The typical error of metallicity for KD02 (all star forming), KD02 (pairs), D02 (all star forming), D02 (pairs) are 0.010, 0.011, 0.009, 0.009, respectively, which are small enough to impact the final results. We divide the stellar masses into 10 bins and calculate the median value of metallicity in each bin. Then we interpolate these 10 points to obtain the best-fitting mass–metallicity relationship by using the 'SCIPY.INTERPOLATE.INTERP1D'[2] function from PYTHON. This relationship is shown in Fig. 2.

We aim to find out whether the sharing CGM of pairs will reduce the metallicity difference between them or not. Thus, we here calculate the metallicity difference between two members in a

[2]https://docs.scipy.org/doc/scipy/reference/generated/scipy.interpolate.interp1d.html

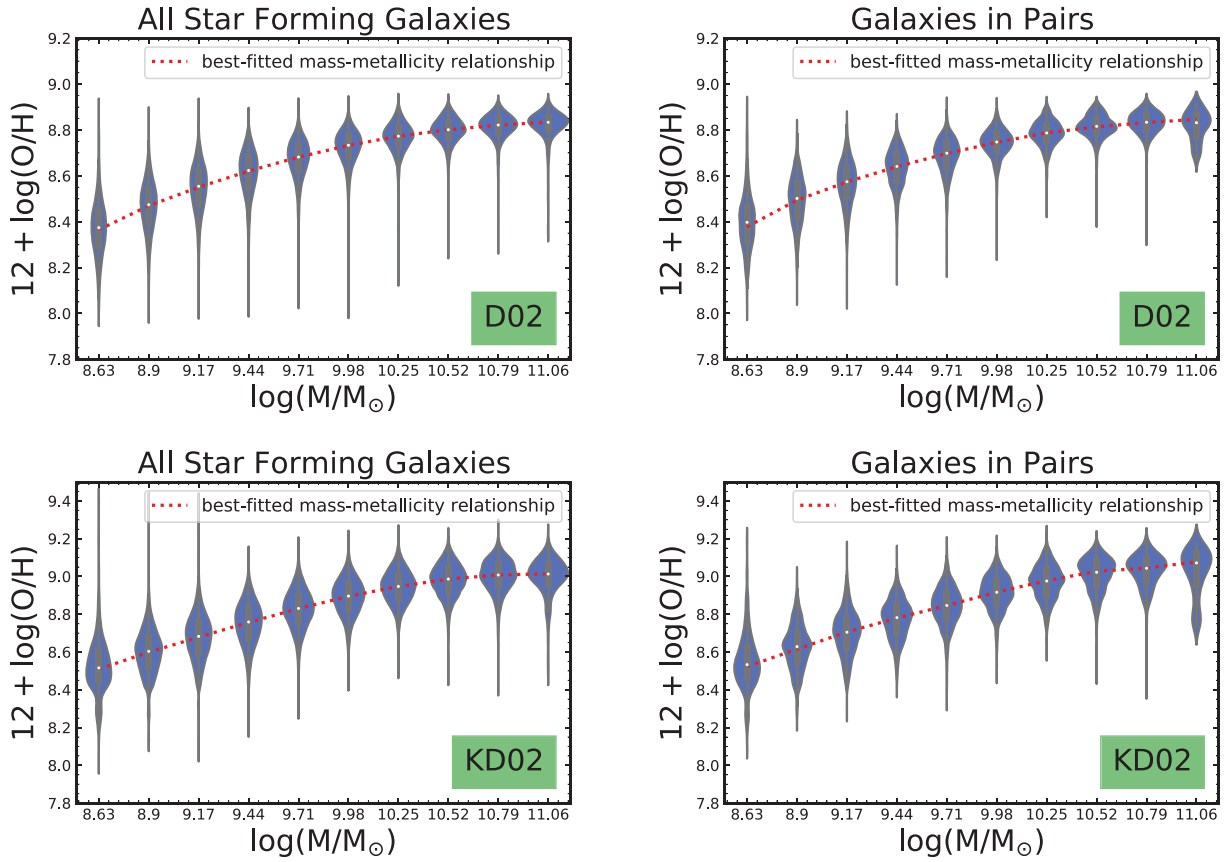

Figure 2. Violin plots illustrate the probability distribution of metallicity in each stellar mass bin in the stellar mass–metallicity relationship of SF galaxies from SDSS DR7. In the violin plot, the white spot, the thick black bars, the thin black bars, the thin black lines in each bin represent the median value, the interquartile range, 1.5 × interquartile range, the distribution of y-axis data, respectively. The metallicity indicator in the top, the bottom panel are from D02, KD02, respectively. The left-hand, right-hand panels represent the relationship for all SF galaxies, pairs (SF–SF pairs and SF–passive pairs), respectively. All SF galaxies contains pairs and the control galaxies. The red dotted lines represent the 'best-fitting mass–metallicity relationship'.

galaxy pair and compare them to two-fake pair galaxies from control samples that have the same stellar masses and redshift as the observed one but not physically associated. The metallicity difference between two members in pairs (SF–SF pairs) is simply defined as:

$$\Delta\log(\mathrm{O/H})_{\mathrm{diff}} = \mathrm{Z_{pri}} - \mathrm{Z_{sec}}, \quad (4)$$

where $\mathrm{Z_{pri}}$ is the metallicity measured from strong emission line of galaxies in pairs (or 'fake' pairs) with higher stellar mass and $\mathrm{Z_{sec}}$ the metallicity from the lower one. The sharing CGM likely decreases the metallicity difference between two members in pairs because gas in two galaxies are contaminated by a common bulk of CGM. If $|\Delta\log(\mathrm{O/H})_{\mathrm{diff,fake}}| > |\Delta\log(\mathrm{O/H})_{\mathrm{diff,real}}|$, we consider the share of the CGM between pairs decreases the metallicity difference between two members in pairs.

As shown in the top two left-hand panels of Fig. 3, for both metallicity indicators, there is no significant difference in the distribution between pairs and control galaxies. Table 2 provides additional statistics of those parameters. If the CGMs affect the distribution of metals between pairs, compared to the isolated fake pairs from control samples, we expect a smaller distribution difference between pairs, such as the mean and 1σ of $\Delta\log(\mathrm{O/H})_{\mathrm{diff}}$. However, compared to the span of the $\Delta\log(\mathrm{O/H})_{\mathrm{diff}}$ ($\approx$ 1.4 or 2.0)), the difference of mean value ($\approx$0.1150 for D02, $\approx$0.1267 for KD02) and 1σ ($\approx$0.1380 for D02, $\approx$0.1622 for KD02) between pairs and control samples are too small to be important. Thus, no significant difference is found in the $\Delta\log(\mathrm{O/H})_{\mathrm{diff}}$ between pairs and control samples, which means that the share of CGM will not reduce the metallicity difference between pairs.

Then we analyse the metallicity offset from the best-fitting stellar mass–metallicity relationship of galaxies in pairs ($\Delta\log(\mathrm{O/H})_{\mathrm{MS}}$), which is:

$$\Delta\log(\mathrm{O/H})_{\mathrm{MS}} = \mathrm{Z} - \mathrm{f}(\mathrm{M}_\star), \quad (5)$$

where Z is the metallicity of each galaxy and $\mathrm{f}(\mathrm{M}_\star)$ is the metallicity of a galaxy with the same stellar mass but on the main sequence. The distribution is shown in the two bottom left panels in Fig. 3. Table 3 also displays the statistics of unweighted metallicity difference. For D02, the mean $\Delta\log(\mathrm{O/H})_{\mathrm{MS}}$ of pairs (0.0113) is larger than that of control samples (0.0066). Overall, the difference between pairs and control samples is still too small to be significant. In this way, we conclude that there is no significant difference in $\Delta\log(\mathrm{O/H})_{\mathrm{MS}}$ between pairs and control galaxies.

We also use the violin plots to analyse the parameters that might influence the distribution of $\Delta\log(\mathrm{O/H})_{\mathrm{diff}}$, such as stellar mass ratio, SFR, and sSFR, as shown in Fig. 4. An additional requirement is included: the pairs and control samples should have similar SFR, sSFR (0.1 dex) for the left-hand and middle panels, respectively. There is no significant difference between the distribution of pairs and control samples in each panel, which means that the SFR, sSFR, and stellar mass might not significantly change the $\Delta\log(\mathrm{O/H})_{\mathrm{diff}}$ be-

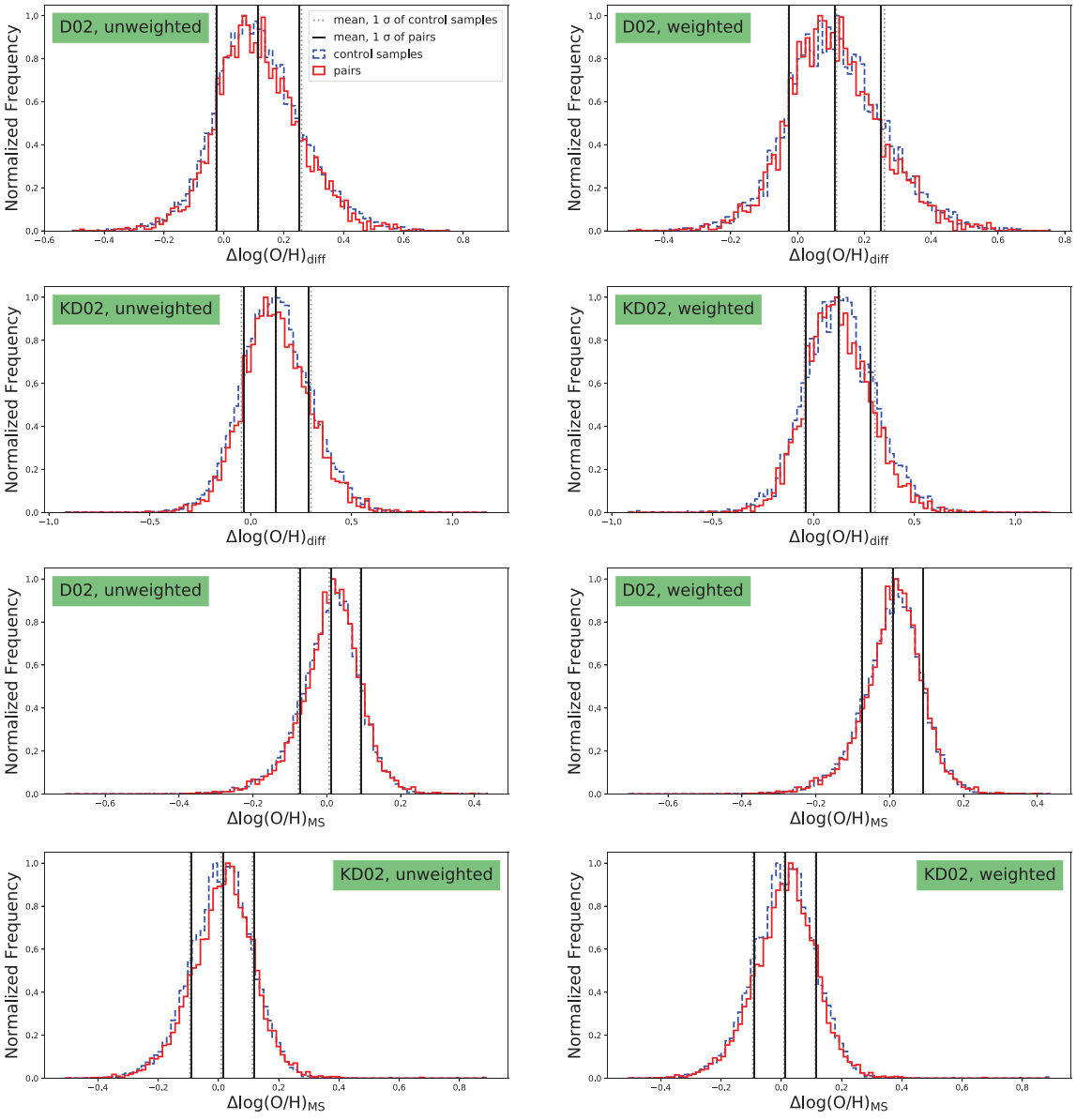

Figure 3. The distribution of $\Delta\log(O/H)_{diff}$ and $\Delta\log(O/H)_{MS}$ with different metallicity indicators are shown in this figure. The left-hand panels represent the unweighted data, and the right-hand panels represent the weight corrected data. The red solid lines are pair galaxies, the blue dashed are control galaxies. The vertical black solid line, grey dashed line illustrates the mean and 1σ of control samples, pairs, respectively. The metallicity indicator for the first and third rows are from D02, the rest of rows are from KD02.

Table 2. Unweighted and weighted $\Delta\log(O/H)_{diff}$.

Metallicity indicator	Type	Weight	$\Delta\log(O/H)_{diff}$ Mean	1σ
D02	Pairs	NO	0.1150	0.1380
		YES	0.1116	0.1373
	Control samples	NO	0.1157	0.1437
		YES	0.1166	0.1436
KD02	Pairs	NO	0.1267	0.1622
		YES	0.1229	0.1604
	Control samples	NO	0.1265	0.1722
		YES	0.1295	0.1750

Table 3. Unweighted and weighted $\Delta\log(O/H)_{MS}$.

Metallicity indicator	Type	Weight	$\Delta\log(O/H)_{MS}$ Mean	1σ
D02	Pairs	NO	0.0113	0.0825
		YES	0.0087	0.0827
	Control samples	NO	0.0066	0.0834
		YES	0.0063	0.0837
KD02	Pairs	NO	0.0157	0.1041
		YES	0.0130	0.1036
	Control samples	NO	0.0091	0.1039
		YES	0.0092	0.1039

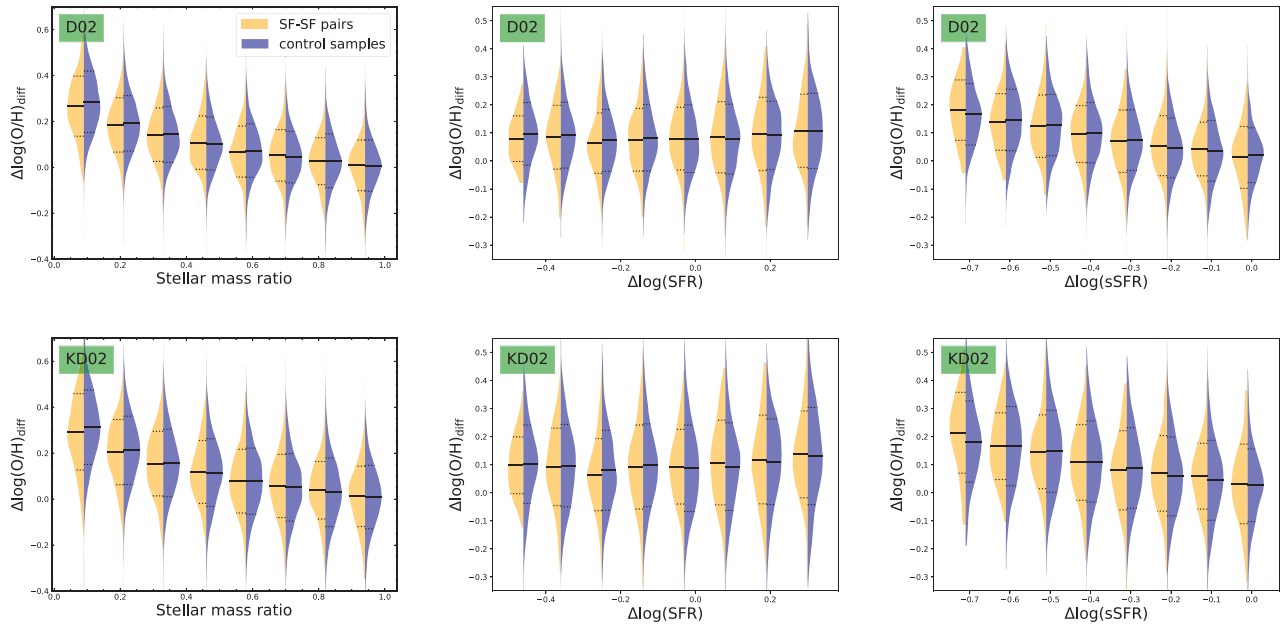

Figure 4. Violin plots show the probability distribution of $\Delta\log(O/H)_{diff}$ for SF–SF pairs compared to control samples for the stellar mass ratio, $\Delta\log(SFR)$, and $\Delta\log(sSFR)$. The horizontal solid lines, dotted lines represent the median value, the 1σ confidential intervals in each bin, respectively. The top, bottom panels represent the metallicity indicator of D02, KD02, respectively.

tween control samples and pairs. A slight increase of $\Delta\log(O/H)_{diff}$ with an increase of $\Delta\log(SFR)$ can be found in the left two panels. For the right four panels, a slight negative trend can be found in the relationship between $\Delta\log(O/H)_{diff}$ and $\Delta\log(sSFR)$, and $\Delta\log(O/H)_{diff}$ and the stellar mass ratio. Overall, the SFR difference, the sSFR difference, and the stellar mass ratio are found not to influence the $\Delta\log(O/H)_{diff}$ between pairs and control samples.

The trend of $\Delta\log(O/H)_{MS}$ and $\Delta\log(O/H)_{diff}$ as a function of the projected separation is further used to investigate whether the separation between pairs impacts the metallicity distribution. The closer the two galaxies, the larger area of sharing the CGM. We expect to see that the projected distance between pairs might influence the metallicity distribution. In the top panels of Fig. 5, the median value of $\Delta\log(O/H)_{MS}$ for pairs is smaller than that of control samples, when the projected distances are smaller than 150 kpc. However, in the bottom panels, no evidence shows the difference of $\Delta\log(O/H)_{diff}$ between pairs and control samples. Compared to previous work (e.g. Scudder et al. (2012), Ellison et al. (2013), Bustamante et al. (2020)) that found metallicity dilution, no significant metallicity dilution is found in this work. This difference is caused by the different definition of control samples (Section 4.2 in detail). Because the more massive galaxies contain more metal, the median value of $\Delta\log(O/H)_{diff}$ is greater than zero. However, there is no obvious trend of change as a function of the projected distance.

4 DISCUSSION

4.1 Incompleteness

Due to the incompleteness, we might lose some pairs in our sample and thus obtain a biased result. The incompleteness of data is caused by the flux limit of the survey and the fiber collision effect (Patton et al. 2016). In this part, we will discuss the influence of incompleteness on the results.

First, for the flux limit of the SDSS survey, we separately analyse the distribution of the Petrosian r band magnitude for pairs and control samples. In Fig. 6, the r band distribution of these two sets is quite similar. However, the distribution of redshift shows that there are more control samples lies between 0.05 and 0.2 than pairs. A weighting scheme in §2 is introduced to reduce the difference. Even though, the overall distribution of Petrosian r band magnitude between pairs and control samples is similar because of the selection requirement. However, a small difference exist in redshift distribution between pairs and control sample. Thus, the incompleteness caused by the flux limit of the survey of control samples and matched pairs is similar.

Secondly, the existence of the physical separation of fibers will make some pair galaxies missed if they are located out of the fiber. The phenomenon that pairs appear in the photometric data but not in the spectroscopic data is called spectroscopic incompleteness. For SDSS, the fiber separation is 55 arcsec (Blanton et al. 2003; Patton et al. 2016). Patton & Atfield (2008) found that the ratio of the spectroscopic to photometric pairs at angular distance $\geq$ 55 arcsec is 37.5 per cent of that at angular distance $\leq$ 55 arcsec. Thus, for pairs whose the projected distances are less than 55 arcsec, we use a weight scheme $w_\theta = 3.08$ to correct this selection effect (Bustamante et al. 2020).

As seen in Fig. 3, there is no significant difference between the left-hand (unweighted) and the right-hand (weighted) panels. Table 2 and 3 present a quantitative comparison. In this case, we find that the incompleteness introduced by fiber collision does not significantly influence the results.

4.2 The effects of different control samples

For $\Delta\log(O/H)_{MS}$, the different definition of control samples will influence the final result. Here, we compare our result with that from

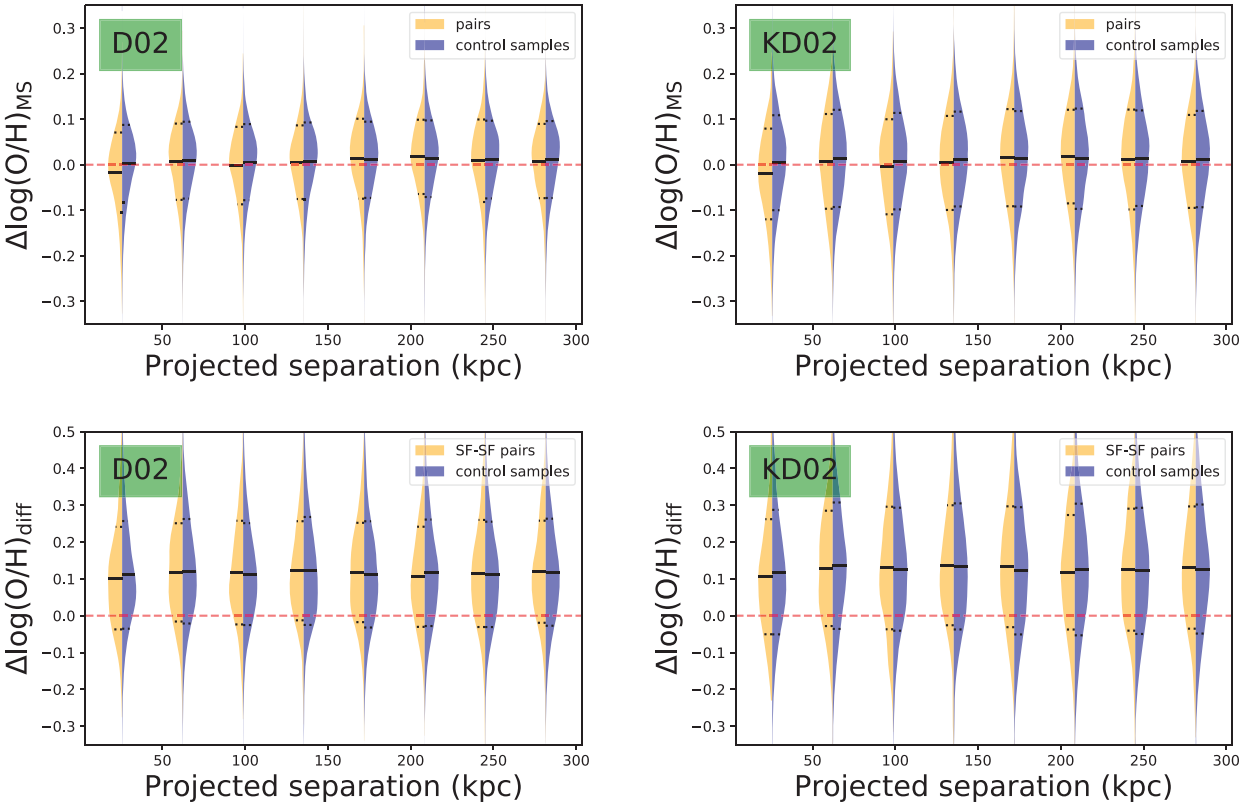

Figure 5. Violin plots show the probability distribution of $\Delta\log(O/H)_{MS}$, $\Delta\log(O/H)_{diff}$ for both SF–SF pairs and SF–passive pairs, SF–SF pairs, respectively, compared to control samples for the projected separation. In the violin plot, the white spot, the thick black bars, the thin black bars, the thin black lines in each bin represent the median value, the interquartile range, 1.5 × interquartile range, the distribution of y-axis data, respectively. The metallicity indicator in the left-hand, the right-hand panel are from D02, KD02, respectively. The red horizon line in each panel represents the y-axis data equals to zero.

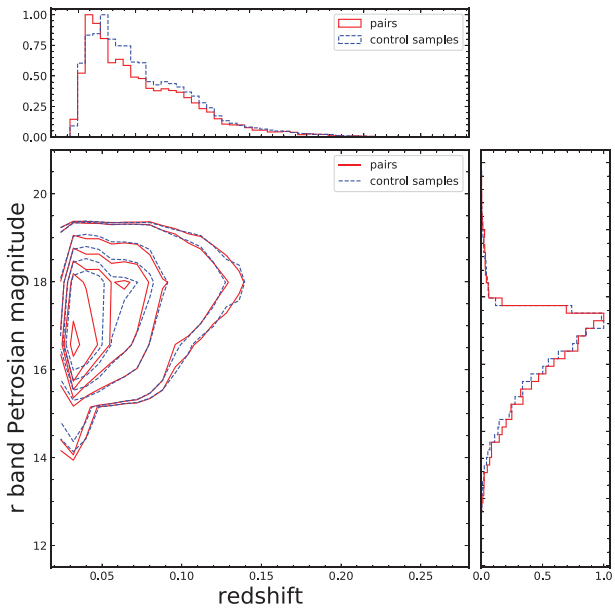

Figure 6. The relationship between redshift and r band Petrosian magnitude. The horizontal and vertical histogram represents the distribution of redshift and the r band magnitude, respectively.

Scudder et al. (2012), which used the following equation:

$$\Delta\log(O/H) = 12 + \log(O/H)_{pair} - \text{median}(12 + \log(O/H)_{control}), \quad (6)$$

where $\text{median}((12 + \log(O/H))_{control})$ is the median value of control samples for each pair galaxy. Because equation (6) directly compares the metallicity between pairs and their matched control samples, we compare the metallicity of pairs with the median value of metallicity in each stellar mass bin of control samples. We find obvious metallicity dilution when the projected distance is smaller than 150 kpc, as shown in the top panels of Fig. 7.

We also plot the $\Delta\log(O/H)_{MS}$ using the function from Bustamante et al. (2020), which use the fundamental metallicity relation (FMR). The FMR describes the relationship between the stellar mass, metallicity, and SFR. In the bottom panels of the Fig. 7, we find the metallicity dilution as a function of the projected distance too.

Therefore, the definition of control samples typically affect the result of $\Delta\log(O/H)_{MS}$.

4.3 Physical mechanism

No significant evidence is found in this paper that shows the sharing CGM will reduce the metallicity difference between pairs. This means that the sharing CGMs has a little measurable impact on regulating the metallicity of pairs. This agrees with the result from Genel (2016) that the CGM metallicity has little effect on the metallicity in the galaxies. In this way, even with sharing CGMs that

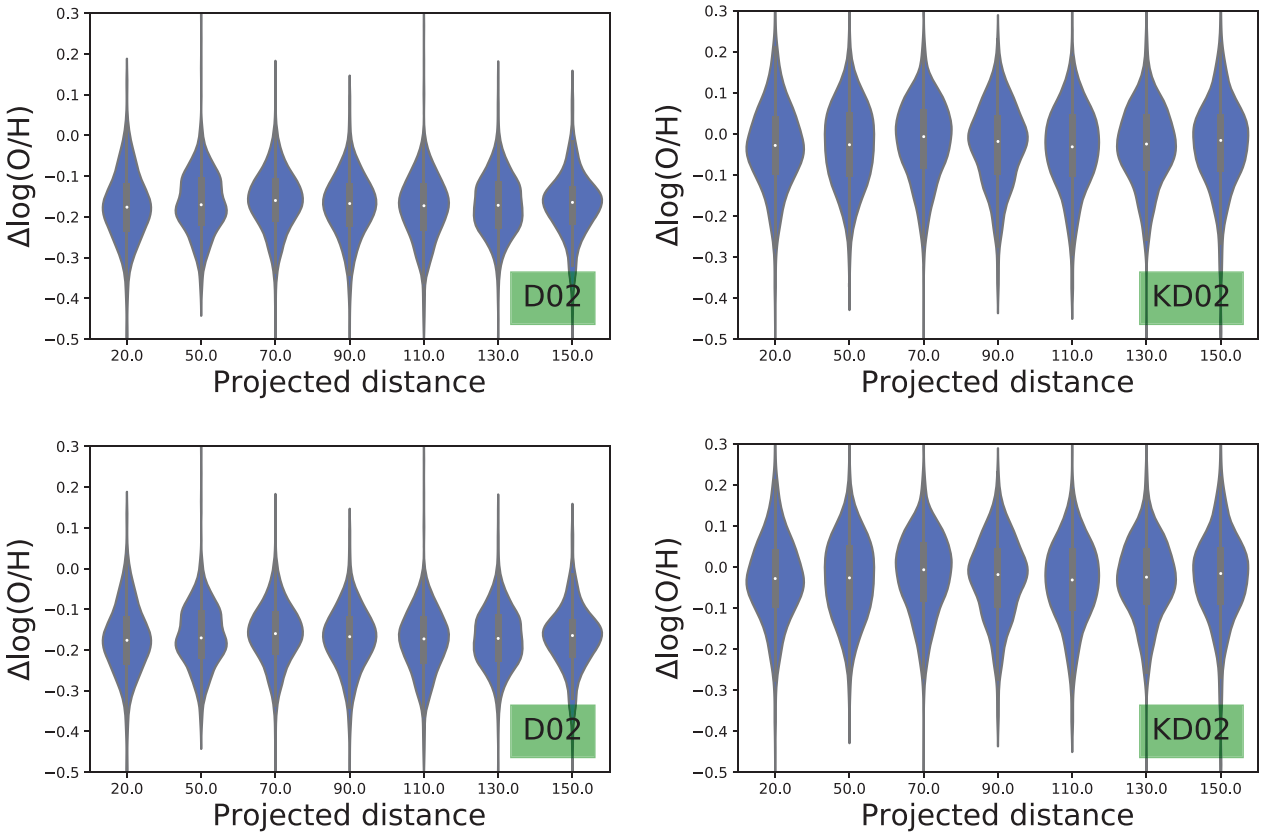

Figure 7. The relationship between Δlog(O/H) and the projected distance. The Δlog(O/H) in the top panels are calculated by using equation (6). The Δlog(O/H) in the bottom panels are calculated by using the FMR from Bustamante et al. (2020).

may mix and regulate the metal distribution in the CGMs between pairs, the change in the CGMs may not influence the metallicities within galaxies. In addition, as shown in Péroux et al. (2020), Wendt et al. (2021), the metallicity distribution in the CGM is uneven: more metals located along the minor axis than the major axis of galaxy. Outflows that transport the metal-rich gas into the CGM, usually locate along the minor axis. Inflows can contain the metal-poor gas, usually locate along the major axis. As a result, the axis along which CGM is shared may fluctuate the metallicity dilution effects.

Compared to isolated galaxies, pairs have an additional way to affect the distribution of gas between each other. When galaxies begin to approach, they will first share the CGM and then have interaction with each other. Previous studies (Ellison et al. 2008; Bustamante et al. 2020) show that the interaction between pairs will dilute the gas and enhance the star formation. In this work, we expect to find the galaxies in pairs that have CGM sharing. So we redefine galaxy pairs to allow them to have a larger separation than that of pairs from previous works. Therefore, there exists an area where galaxies have CGM sharing but without interaction, which is shown in Table 1.

In Fig. 8, when the projected distance ≤ 150 kpc, the $\Delta\log(O/H)_{MS}$ of SF–SF pairs are smaller than that of SF–passive pairs in each separation bin, which shows that the interaction triggers the metal-poor gas from the sharing CGM to dilute metals within galaxies. When the projected distance ≥ 150 kpc, there is no significant difference in $\Delta\log(O/H)_{MS}$ between SF–SF pairs and SF–passive pairs, which means that only the sharing CGM itself, without the galaxy interaction, don't have the possibility to affect the metal distribution between pairs. Because the majority of the SF–passive pairs are minor mergers, we add a stellar mass ratio cut on SF–SF pairs. The result doesn't change, so we think it is valid in the minor merger case. This again proves that the sharing of CGM without interactions may not impact the central metallicity of galaxies.

5 CONCLUSIONS

In this work, we select SF galaxies with strong emission lines and explore the MZR of pair galaxies using single fiber data from SDSS DR7. To study the effect of CGM on regulating the star formation and the metal re-distribution process, pairs are defined to have separations of less than 300 kpc. A weighting scheme is introduced to correct the select effect from flux limit and fiber collision. The main results are shown below:

(1) The MZR trend is similar to Tremonti et al. (2004): the monotonic correlation between stellar mass-metallicity and the trend becomes flat when stellar mass is higher than $10^{10.5}$ $M_{\odot}$.

(2) Compared to control samples, there is no significant difference in the distribution of metallicity offset from the best-fitting stellar mass–metallicity relationship of galaxies in SF–SF pairs ($\Delta\log(O/H)_{MS}$), metallicity difference between two members in pairs ($\Delta\log(O/H)_{diff}$, both SF–SF and SF–Passive pairs), which means that the CGM will not decrease the metallicity difference within 3 arcsec region of pairs.

(3) The parameters such as the stellar mass ratio, SFR, and sSFR are found not to impact $\Delta\log(O/H)_{MS}$ and $\Delta\log(O/H)_{diff}$ between pairs.

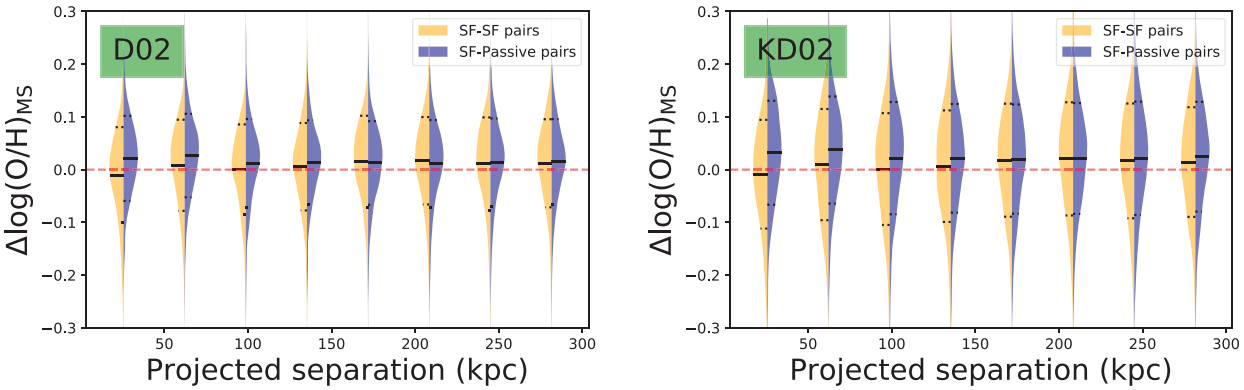

Figure 8. Violin plots show the probability distribution of $\Delta\log(O/H)_{MS}$ for SF–SF pairs compared to SF–Passive pairs as a function of the projected separation. In the violin plot, the white spot, the thick black bars, the thin black bars, the thin black lines in each bin represent the median value, the interquartile range, 1.5 × interquartile range, the distribution of y-axis data, respectively. The metallicity indicator in the left-hand, the right-hand panel are from D02, KD02, respectively. The red horizon line in each panel represents the y-axis data equals to zero. The orange, blue colour in the picture represent the SF–SF pairs and SF–Passive pairs respectively. The $\Delta\log(O/H)_{MS}$ equal to the metallicity offset from the 'best-fitting' stellar mass–metallicity relationship.

(4) Comparing the $\Delta\log(O/H)_{MS}$ of SF–SF pairs with that of SF–Passive pairs, we find that only with the assistance of galaxy interaction, the sharing CGM can trigger the metal-poor gas fall into the galaxy centre. Because most of the SF–Passive pairs are minor mergers, this result is valid in the minor merger case.

In conclusion, the CGM sharing should not be a major factor that shapes the metal evolution of galaxies. The gas recycling and the uneven distributions of metals in CGMs may fluctuate the effects of sharing CGMs in regulating metallicity of galaxies.

ACKNOWLEDGEMENTS

We thank the referee for a detailed report that significantly improve the presentation of our work. SZ and YS acknowledge the support from the National Key Research and Development Program of China (no. 2017YFA0402704, no. 2018YFA0404502), the National Natural Science Foundation of China (NSFC grants 11825302, 11733002, and 11773013). YS thanks the support from the Tencent Foundation through the XPLORER PRIZE.

DATA AVAILABILITY

This paper makes use of the MPA-JHU DR7 data, which is available at https://wwwmpa.mpa-garching.mpg.de/SDSS/DR7.

REFERENCES

Abazajian K. N. et al., 2009, ApJS, 182, 543
Baldwin J. A., Phillips M. M., Terlevich R., 1981, PASP, 93, 5
Blanc G. A., Lu Y., Benson A., Katsianis A., Barraza M., 2019, ApJ, 877, 6
Blanton M. R., Lin H., Lupton R. H., Maley F. M., Young N., Zehavi I., Loveday J., 2003, AJ, 125, 2276
Brinchmann J., Charlot S., White S. D. M., Tremonti C., Kauffmann G., Heckman T., Brinkmann J., 2004, MNRAS, 351, 1151
Brooks A. M., Governato F., Booth C. M., Willman B., Gardner J. P., Wadsley J., Stinson G., Quinn T., 2007, ApJ, 655, L17
Bustamante S., Ellison S. L., Patton D. R., Sparre M., 2020, MNRAS, 494, 3469
Calura F., Pipino A., Chiappini C., Matteucci F., Maiolino R., 2009, A&A, 504, 373
Calzetti D., Armus L., Bohlin R. C., Kinney A. L., Koornneef J., Storchi-Bergmann T., 2000, ApJ, 533, 682
Chen Y.-M., Tremonti C. A., Heckman T. M., Kauffmann G., Weiner B. J., Brinchmann J., Wang J., 2010, AJ, 140, 445
Chisholm J., Tremonti C., Leitherer C., 2018, MNRAS, 481, 1690
Denicoló G., Terlevich R., Terlevich E., 2002, MNRAS, 330, 69
Ellison S. L., Mendel J. T., Patton D. R., Scudder J. M., 2013, MNRAS, 435, 3627
Ellison S. L., Patton D. R., Simard L., McConnachie A. W., 2008, AJ, 135, 1877
Erb D. K., Shapley A. E., Pettini M., Steidel C. C., Reddy N. A., Adelberger K. L., 2006, ApJ, 644, 813
Finlator K., Davé R., 2008, MNRAS, 385, 2181
Garnett D. R., 2002, ApJ, 581, 1019
Garnett D. R., Kennicutt R. C., Jr, Bresolin F., 2004, ApJ, 607, L21
Genel S., 2016, ApJ, 822, 107
Groves B., Brinchmann J., Walcher C. J., 2012, MNRAS, 419, 1402
Gunn J. E. et al., 2006, AJ, 131, 2332
Heckman T. M., Armus L., Miley G. K., 1990, ApJS, 74, 833
Kauffmannet al., 2003 MNRAS, 341, 33
Kauffmann G. et al., 2003, MNRAS, 346, 1055
Kewley L. J., Dopita M. A., 2002, ApJS, 142, 35
Kewley L. J., Ellison S. L., 2008, ApJ, 681, 1183
Kewley L. J., Geller M. J., Barton E. J., 2006, AJ, 131, 2004
Kewley L. J., Heisler C. A., Dopita M. A., Lumsden S., 2001, ApJS, 132, 37
Kirby E. N., Cohen J. G., Guhathakurta P., Cheng L., Bullock J. S., Gallazzi A., 2013, ApJ, 779, 102
Köppen J., Weidner C., Kroupa P., 2007, MNRAS, 375, 673
Lee H., Skillman E. D., Cannon J. M., Jackson D. C., Gehrz R. D., Polomski E. F., Woodward C. E., 2006, ApJ, 647, 970
Lequeux J., Peimbert M., Rayo J., Serrano A., Torres-Peimbert S., 1979, A&A, 80, 155
Lochhaas C., Bryan G. L., Li Y., Li M., Fielding D., 2020, MNRAS, 493, 1461
Ly C., Malkan M. A., Rigby J. R., Nagao T., 2016, ApJ, 828, 67
Mannucci F., Cresci G., Maiolino R., Marconi A., Gnerucci A., 2010, MNRAS, 408, 2115
Mathis J. S., 1990, ARA&A, 28, 37
Ma X., Hopkins P. F., Faucher-Giguère C.-A., Zolman N., Muratov A. L., Kereš D., Quataert E., 2015, MNRAS, 456, 2140
Onodera M. et al., 2016, ApJ, 822, 42
Pan H.-A. et al., 2018, ApJ, 868, 132

Patton D. R., Atfield J. E., 2008, ApJ, 685, 235
Patton D. R., Qamar F. D., Ellison S. L., Bluck A. F. L., Simard L., Mendel J. T., Moreno J., Torrey P., 2016, MNRAS, 461, 2589
Peng Y.-j., Maiolino R., 2014, MNRAS, 438, 262
Péroux C., Nelson D., van de Voort F., Pillepich A., Marinacci F., Vogelsberger M., Hernquist L., 2020, MNRAS, 499, 2462
Planck Collaboration XIII, 2016, A&A, 594, A13
Salimet al., 2007 ApJS, 173, 267
Sanders R. L. et al., 2018, ApJ, 858, 99
Savaglio S. et al., 2005, ApJ, 635, 260
Scudder J. M., Ellison S. L., Torrey P., Patton D. R., Mendel J. T., 2012, MNRAS, 426, 549
Steidel C. C., Erb D. K., Shapley A. E., Pettini M., Reddy N., Bogosavljević M., Rudie G. C., Rakic O., 2010, ApJ, 717, 289
Tremonti C. A. et al., 2004, ApJ, 613, 898
Troncoso P. et al., 2014, A&A, 563, A58
Tumlinson J., Peeples M. S., Werk J. K., 2017, ARAA, 55, 389
Tumlinson J. et al., 2011, Science, 334, 948
Weiner B. J. et al., 2009, ApJ, 692, 187
Wendt M., Bouché N. F., Zabl J., Schroetter I., Muzahid S., 2021, MNRAS, 502, 3733
Werk J. K. et al., 2014, ApJ, 792, 8
Wilde M. C. et al., 2020, preprint (arXiv:2008.08092)
Wilson T. J. et al., 2019, ApJ, 874, 18
Yabe K. et al., 2014, MNRAS, 437, 3647
York D. G. et al., 2000, AJ, 120, 1579
Zahid H. J., Kewley L. J., Bresolin F., 2011, ApJ, 730, 137

This paper has been typeset from a TEX/LATEX file prepared by the author.